Journal of Infrared, Millimeter, and Terahertz Waves

Modeling of Field Effect Transistor channel as a Nonlinear Transmission Line for Terahertz Detection

--Manuscript Draft--

Manuscript Number:	
Full Title:	Modeling of Field Effect Transistor channel as a Nonlinear Transmission Line for Terahertz Detection
Article Type:	Devices
Keywords:	Terahertz; High electron mobility transistor; Detector; model; nonlinear transmission line
Corresponding Author:	Nihal Ibrahim, MSc. Faculty of Engineering, Cairo University Giza, Giza EGYPT
Corresponding Author Secondary Information:	
Corresponding Author's Institution:	Faculty of Engineering, Cairo University
Corresponding Author's Secondary Institution:	
First Author:	Nihal Ibrahim, MSc.
First Author Secondary Information:	
Order of Authors:	Nihal Ibrahim, MSc.
	Nadia H. Rafat, PhD
	Salah E.A. Elnahwy, PhD
Order of Authors Secondary Information:	
Abstract:	This paper revisits the theory of operation of field effect transistor in the extremely high frequency scale, where the analysis has gone beyond the conventional cutoff frequency of the transistor. In this range, which is typically the terahertz (THz) and sub-terahertz range, the transistor blocks the high frequency signal and generates a rectified signal related to the input high frequency signal. An analytical model is derived for the channel of the FET in the linear mode of operation in non-resonant THz detection conditions. A transmission line distributed circuit model is applied. This is, from the authors' point of view, the suitable model for high frequency non-quasi static operation and the characteristic parameters of this model are derived from the differential equation governing the electron gas in the channel. A comparison is presented for the calculated photoresponse with previously published experimental one showing good agreement away from the threshold potential. Finally, the effects of coupling between the present model and the external input circuit have been taken into account including the loading effects of the antenna and a discussion is given for the effect on frequency selectivity of the FET.

Modeling of Field Effect Transistor channel as a Nonlinear Transmission Line for Terahertz Detection

Nihal Y. Ibrahim, Nadia H. Rafat, Salah E. A. Elnahwy

Abstract This paper revisits the theory of operation of field effect transistor in the extremely high frequency scale, where the analysis has gone beyond the conventional cutoff frequency of the transistor. In this range, which is typically the terahertz (THz) and sub-terahertz range, the transistor blocks the high frequency signal and generates a rectified signal related to the input high frequency signal. An analytical model is derived for the channel of the FET in the linear mode of operation in non-resonant THz detection conditions. A transmission line distributed circuit model is applied. This is, from the authors' point of view, the suitable model for high frequency non-quasi static operation and the characteristic parameters of this model are derived from the differential equation governing the electron gas in the channel. A comparison is presented for the calculated photoresponse with previously published experimental one showing good agreement away from the threshold potential. Finally, the effects of coupling between the present model and the external input circuit have been taken into account including the loading effects of the antenna and a discussion is given for the effect on frequency selectivity of the FET.

N. Y. Ibrahim (✉), N. H. Rafat, S. E. A. Elnahwy
Department of Engineering Physics and Mathematics,
Faculty of Engineering,
Cairo University.
e-mail: nihal_eng@yahoo.com

Introduction

The use of Field Effect Transistor (FET) for Terahertz (THz) signal detection beyond its transit-time cut-off frequency, f_s, has sparked increasing attention lately [1]. The phenomena can be explained with the simultaneous nonlinear modulation of the carrier density and velocity of the 2-dimensional electron plasma in the transistor channel excited by the incoming THz radiation. THz electric field is rectified, like in square law detectors, and a constant (DC) source-to-drain voltage appears. This voltage is the detection signal and is called the photovoltaic response or the photoresponse. This can be calculated by solving the appropriate differential equation with appropriate boundary conditions. More details about the detection mechanism can be found in the literature [2].

Existing theories distinguish between two main cases: First, the resonant case where plasmons decay slowly compared to the period of the operating frequency, allowing for plasma resonances. Plasmons may oscillate under the gate, which serves as plasmonic cavity. This case typically requires low temperatures [3],[4] or extremely small device dimensions for operation at room temperature [5] .Second, the non-resonant case of fast decay of plasmons where they are over damped. This is the most important scenario for room-temperature THz detection with FETs with relatively longer channel lengths.

Different kinds of FETs, like GaAs high electron mobility transistors (HEMTs) [6], GaN HEMTs [7], InGaAs HEMTs [8], or silicon metal-oxide-semiconductor (MOSFETs) [9], with a gate length of the order of hundreds of nanometers exhibit good broadband responsivities for the THz radiation. From the point of view of applications, the silicon MOSFETs are the most important ones due to low production costs and ease of integration in electrical circuits. Recently, the first imaging experiments with GaAs FETs [10] and with focal plane arrays made in silicon complementary metal-oxide-semiconductor (CMOS) technology have been reported [11],[12],[13].

This work discusses modeling the broadband detection of FET in the linear region of operation working beyond its cutoff frequency using a non-quasi static model. A model is presented for the channel as a transmission line with nonlinear distributed elements with nonlinear characteristics extracted from the channel's characteristics in the linear region of operation. A discussion is given for how this model affects the input coupling efficiency, and hence the frequency rolls off due to input RC constant. The results are compared with exiting experimental data to show a good match away from the threshold point.

Non-quasi-static modeling of FET

Analytical or semi-analytical MOSFET models are usually based on the so-called gradual channel approximation (GCA). The GCA assumes that, under certain conditions, the electrostatic problem of the gate region can be expressed in terms of two coupled one-dimensional equations; Poisson's equation for determining the vertical charge density profile under the gate and a charge transport equation for the channel. This allows determining self-consistently both the channel potential and the charge profile at any position along the gate. A direct inspection of the two-dimensional Poisson's equation for the channel region shows that the GCA is valid if it can be assumed that the electric field gradient in the lateral direction of the channel is much less than that in the vertical direction perpendicular to the channel[14].

Typically, the authors find that the GCA is valid for long-channel MOSFETs where the ratio between the gate length and the vertical distance of the space charge region from the gate electrode, the so-called aspect ratio, is large. However, if the MOSFET is biased in saturation the GCA always becomes invalid near drain as a result of the large lateral field gradient that develops in this region. The GCA fails also at very high operation frequencies since the lateral variation gradient increases rapidly compared to vertical potential variations.

Most of the MOSFET models used in SPICE are based on the quasi-static assumption (QSA), in which an instantaneous charging of the inversion layer is assumed. In QSA, the distributed gate-channel capacitance is lumped into discrete capacitances between the gate, source and drain nodes, ignoring the finite charging time arising from the *RC* product associated with the channel resistance and the gate-channel capacitance. For very high-frequency operation of the MOSFET, comparable to the inverse carrier transport time of the channel (non-quasi-static (NQS) regime), the temporal relaxation of the inversion and depletion charges has to be considered. Hence, QSA based circuit simulations fails to accurately predict the performance of high-speed circuits. The schematic of the basic FET is represented in Fig. 1 where the varying thickness of the channel represents the varying potential along the channel which results in varying electron concentration as well as varying resistance along the channel.

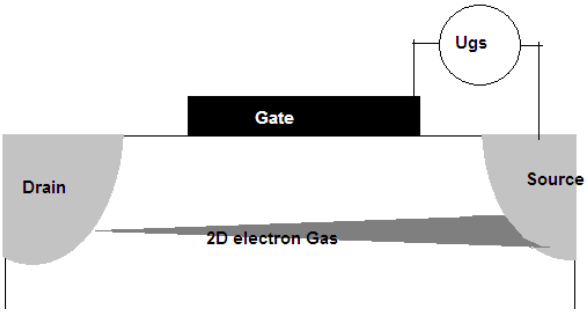

Fig. 1 Schematic diagram of HEMT with illustration of the 2DEG (Channel) potential in linear region

The actual channel of a MOSFET is analogous to a distributed *RC* network with an equivalent circuit as illustrated in Fig. 2. The basic model used is that of a transmission line consisting of the gate metal and the 2DEG channel. The biases related to the device are $U_{gs}=U_{GS}-V_{th}$ for the gate to source bias with respect to the threshold bias and $U_{cs}(x)$ for the bias along the channel relative to the source, where x represents the position along the channel starting from the source at $x=0$ and ending at the drain at $x=L$ (L=channel length).

Derivation of the Characteristic Model Parameters

For the most general case, the channel transmission line (TL) model would include an inductance (plasma-resonant case) and a parasitic conductance parallel to the gate capacitor (leaky gate) as well as the gate capacitance and the channel resistance. The telegrapher's equations provide solutions for the applied potential signal $U^{TL}(x)$ and current $I^{TL}(x)$ along the transmission line of the gated region. These are:

$$\frac{\partial U^{TL}(x,t)}{\partial x} = -r_0 I^{TL}(x,t) - l_0 \frac{\partial I^{TL}(x,t)}{\partial t} \quad (1)$$

$$\frac{\partial I^{TL}(x,t)}{\partial x} = -g_0 U^{TL}(x,t) - c_0 \frac{\partial U^{TL}(x,t)}{\partial t} \quad (2)$$

Where the lower-case letters are the transmission-line parameters per unit length, l_0 the inductance per unit length, g_0 the gate-channel (leakage) conductance per unit length, r_0 the channel resistance (losses) per unit length, c_0 *is* the gate capacitance per unit length. $c_0=\varepsilon_0\varepsilon_r W/d=c_G/L$, with W and d the width and depth of the channel respectively, and C_G the total gate capacitance.

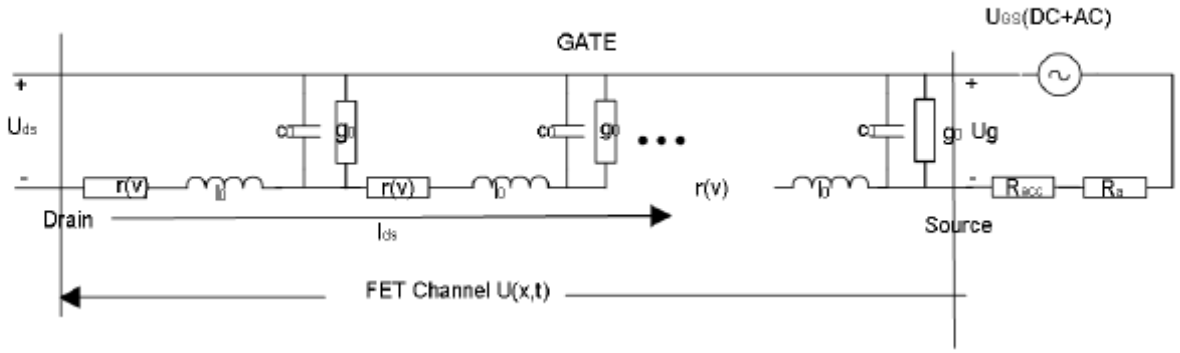

Fig. 2 Circuit diagram of the suggested FET channel as a Transmission Line

Since the case of nonresonant detection in transistors with long gates is being treated here, the characteristic relation $\omega\tau<<1$ is valid, where τ is the momentum relaxation time of the plasmons in the channel. The inductance, l_0 includes the (momentum) relaxation time of the plasmons through the channel such that the plasmon decay time is given by $\tau = l_0/r_0$. For the non-resonant case, $\omega\tau = \omega\, l_0/r_0<<1$ hence the inductance can be neglected. Furthermore, the gate is assumed to be non-leaky, i.e. $g_0=0$.

Although it has been assumed that the channel resistivity can be taken as constant [15], the actual channel resistance is not uniformly distributed along the channel as previously assumed. It actually depends, nonlinearly, on the channel capacitance and the potential distribution along the channel. This means that the applied bias and the operation point will affect the channel performance. For a more general description of the channel one looks at the basic transmission line equation taking into consideration that $U^{TL}=U_{gc}$ which is the gate to channel potential and $I^{TL}=-I_{cs}$ (channel to source current). Rewriting equations 1 and 2, the potential and current along the channel can thus be represented by:

$$\frac{\partial U_{gc}(x,t)}{\partial x} = rI_{cs}(x,t) \qquad 3$$

$$\frac{\partial I_{cs}(x,t)}{\partial x} = c_0\frac{\partial U_{gc}(x,t)}{\partial t} \qquad 4$$

From the basic FET theory, approximated to the linear region of operation, the channel's resistance per unit length can be approximated to:

$$r = \frac{dR}{dx} = -\frac{1}{\mu c_0(U_g - V_{th} - U_{cs}(x,t))} = -\frac{1}{\mu c_0(U_{gc})} \qquad 5$$

Where μ is the charge carrier effective mobility. Substituting (Eq.5) into (Eq.3) and rewriting $Ugc=U_{Gc}-V_{th}=U(x,t)$, where V_{th} is the threshold potential and letting $I_{cs}=I$. we re-write Eq. 3 and 4 as:

$$U(x,t)\frac{\partial U(x,t)}{\partial x} = \frac{1}{2}\frac{\partial U^2(x,t)}{\partial x} = -\frac{I(x,t)}{\mu c_0} \qquad 6$$

$$\frac{\partial I(x,t)}{\partial x} = c_0\frac{\partial U(x,t)}{\partial t} \qquad 7$$

If it is asssumed that the input terahertz signal is coupled to the transistor through the gate bias as a small AC perturbation added to the DC gate bias , the circuit potentials/current can as well be written as DC parts (subscript 0) and AC parts (subscript 1). Hence U_{gs} can be written as $U_{gs}=U_{Gs}-V_{th}=V_{gs0}+V_{gs1}\cos\omega t$. Since the AC signal is small enough second order terms are expected to be vanishingly small and the potential and current can be written as $U(x,t)=V_0(x)+V_1(x)e^{i\omega t}+V^*_1(x)e^{-i\omega t}$, and $I_{cs}(x,t)=\mu c_0 h_0(x)+h_1(x)e^{i\omega t}+h^*_1(x)e^{-i\omega t}$) with higher terms neglected. The above equations can therefore be divided into 2 separate sets of ordinary differential equations as follows:

DC :

$$-2h_0(x) = \frac{d(V_0^2 + 2|V_1|^2)}{dx} \quad (8)$$

$$\frac{dh_0(x)}{dx} = 0 \quad (9)$$

And AC (small signal)

$$-h_1(x) = V_0(x)\frac{dV_1(x)}{dx} + V_1(x)\frac{dV_0(x)}{dx} = \frac{d(V_0(x)V_1(x))}{dx} \quad (10)$$

$$\frac{dh_1(x)}{dx} = i\alpha V_1(x) \quad (11)$$

Where $\alpha=\omega/\mu$,

Assuming the transistor is driven by only DC current (I_D), the boundary conditions are as follows:

$$V_0(0) = V_{gs0}\,,\ h_0(L) = \frac{I_D}{\mu c_0} \quad (12)$$

And $$V_1(0) = 0.5V_{gs1}\,,\ h_1(L) = 0 \quad (13)$$

Solving (Eq. 8 and 9) with BC's in (Eq. 12) one gets

$$V_0^2(x) + 2|V_1(x)|^2 = V_{gs0}^2 + \frac{1}{2}V_{gs1}^2 - \frac{2I_D}{\mu c}x \quad (14)$$

At no applied potential ($V_{gs1}=0$)

$$V_0|_{V_{gs1}=0} = V_{gs0}\sqrt{1 - \frac{2I_D}{\mu c_0 V_{gs0}^2}x} = V_{gs0}\sqrt{1 - \lambda x/L} \quad (15)$$

Where $$\lambda = \frac{2LI_D}{\mu c_0 V_{gs0}^2} = \frac{I_D}{I_{Dsat}} \quad (16)$$

From (Eq. 10 and 11)

$$\frac{d^2(V_0(x)V_1(x))}{dx^2} = -i\alpha V_1(x) \quad (17)$$

By changing the variables of eq. 17 into the function $f=2(V_0(x)V_1(x))/(V_{gs0}V_{gs1})$, letting $y=x/L$, and assuming $V_0(x)\approx V_0|_{Vgs1=0}$ (Eq. 15), one gets:

$$\frac{d^2f}{dy^2} = \frac{-i\alpha L^2}{V_{gs0}\sqrt{1-\lambda y}}f$$

Or

$$\varepsilon^2\frac{d^2f}{dy^2} = \frac{-i}{\sqrt{1-\lambda y}}f \quad (18)$$

where

$$\varepsilon^2 = \frac{V_{gs0}\mu}{\omega L^2} = \frac{L_0^2}{L^2} \text{ for } L_0^2 = \frac{V_{gs0}\mu}{\omega} \quad (19)$$

With boundary conditions (Eq. 12 and 13)

$$f(0) = 1 \quad and\ f'(1) = 0 \quad (20)$$

Physically, L_0 determines a characteristic spatial scale of the decay of the alternating component of voltage, V_1(x) along the channel. Thus, for $\varepsilon<<1$, the oscillations excited at the source do not reach the drain ($L_0<L$ which is equivalent to $\omega_0^2\tau^2<<\omega\tau<<1$.

We can search for solutions of the above equation using the (WKB) approximation, where we obtain two solutions, one of them increases exponentially and the other one decreases exponentially. The boundary conditions allow us to keep only the exponentially decreasing solution, so that,

$$f(y) \simeq (1-\lambda y)^{1/8}\exp\left[\frac{4}{3\sqrt{2}}\frac{(i-1)}{\lambda\varepsilon}\left(1-(1-\lambda y)^{3/4}\right)\right] \quad (21)$$

And

$$h_1(y) = -\frac{V_{gs0}V_{gs1}}{L}\frac{df}{dy} = -\frac{V_{gs0}V_{gs1}}{L}\left\{\frac{-\lambda}{8}(1-\lambda y)^{-7/8} + (1-\lambda y)^{-1/8}\frac{(i-1)}{\sqrt{2}\varepsilon}\right\}\exp\left[\frac{4}{3\sqrt{2}}\frac{(i-1)}{\lambda\varepsilon}\left(1-(1-\lambda y)^{3/4}\right)\right] \quad 22$$

For $\varepsilon<<1$,

$$h_1(y) \approx \frac{V_{gs0}V_{gs1}}{L}(1-\lambda y)^{-1/8}\frac{(1-i)}{\sqrt{2}\varepsilon}\exp\left[\frac{4}{3\sqrt{2}}\frac{(i-1)}{\lambda\varepsilon}\left(1-(1-\lambda y)^{3/4}\right)\right] \quad 23$$

And

$$V_1(y) \approx V_{gs1}\left(1+\frac{3}{8}\lambda y\right)\exp\left[\frac{(i-1)}{\sqrt{2}\varepsilon}y\right] \approx V_{gs1}\exp\left[\frac{(i-1)}{\sqrt{2}\varepsilon}y\right] \quad 24$$

According to this, at $x=L$

$$V_1(1) \approx V_{gs1}\exp\left[\frac{(i-1)}{\sqrt{2}\varepsilon}\right] \approx 0 \quad 25$$

This means that the AC signal vanishes along the channel, and the output will include the DC signal only. The read-out rectification potential at the drain, defined as the increase in the DC output (V_0 at y=1) due to the AC radiation (V_{gs1}), is given by:

$$\delta V_0 = V_0 - V_0|_{V_{gs1}=0} \approx \frac{\frac{1}{2}V_{gs1}^2 - 2|V_1(1)|^2}{2V_{gs0}{}^2\sqrt{1-\lambda}} = \frac{V_{gs1}^2(1)}{4V_{gs0}{}^2\sqrt{1-\lambda}} \quad 26$$

This same result can be obtained by expanding the read-out DC potential V_0in the first order Taylor expansion, $\delta V_0{}^T$ as follows:

$$\delta V_0{}^T = \left.\frac{\partial V_0}{\partial\lambda}\right|_{V_{gs1}=0}\Delta\lambda \quad 27$$

Where,

$$\left.\frac{\partial V_0}{\partial\lambda}\right|_{V_{gs1}=0} = \frac{-V_{gs1}}{2\sqrt{1-\lambda}} \text{ and } \Delta\lambda = \lambda - \lambda|_{V_{gs1}=0} = -\frac{1}{2}V_{gs1}^2 \quad 28$$

This is consistent with the results in [16] and apart from a factor of 4 consistent with the results in [15].

Results and Discussion

As mentioned above, L_0 determines a characteristic spatial scale of the decay of the alternating component of voltage, V_1 along the channel. To test this assumption, the value of the AC signal at L_0 has to be investigated. At x= L_0 and y= $L_0/L = \varepsilon$, the value of V_1 is:

$$V_1(\varepsilon) = V_{gs1}(1-\lambda\varepsilon)^{-3/8}\exp\left[\frac{4}{3\sqrt{2}}\frac{(i-1)}{\lambda\varepsilon}\left(1-(1-\lambda\varepsilon)^{3/4}\right)\right] \approx V_{gs1}(1+{}^3\!/_8\,\lambda\varepsilon)\exp\left[\frac{4}{3\sqrt{2}}\frac{(i-1)}{\lambda\varepsilon}({}^3\!/_4\,\lambda\varepsilon)\right] = V_{gs1}\exp\left[\frac{(i-1)}{\sqrt{2}}\right] \quad 29$$

This means that at L_0 the AC signal has dropped to about one quarter of the induced input value V_{gs1}. Since L is much greater than L_0 the value of the AC signal at the drain is vanishingly small and only the rectified DC signal propagates to the drain terminal. This is consistent with the results in [17]. It is, therefore, safe to consider L_0 as the effective length for the decay of the AC terahertz waves in the FET channel. A safe condition for the validity of the above analysis is, therefore, $L>>L_0$.

The above results are also consistent with the assumed boundary conditions in (Eq.12 and 13). This means that as long as $L>>L_0$, no AC potential/current propagates out of the drain for any applied biasing conditions (i.e. current or voltage driven FET). The main difference between the two cases would be in the expression used in the calculation of λ and whether I_d is driven or dependent on the applied drain potential V_{ds} according to the FET characteristics. It is therefore straight forward to extract the required operation point data (λ) from the FET I-V characteristics (regardless of the details of the experimental setup and boundary conditions). Figure (3) shows a comparison between the experimental data of photoresponse and the results of the theoretical photoresponse (Eq. 26) where λ was calculated using the experimental I-V characteristics of the same HEMT transistor [18]. The results show very good agreement away from the threshold potential.

Two operation points exist with special importance, the first being the threshold point where $V_{gs0}=V_{GS0}-V_{th}\approx 0$, where coupling efficiency is a maximum as well as the readout potential. However it suffers from higher sensitivity to noise and our model cannot easily calculate the responsivity as thermally activated carriers, the break-up of the 2DEG into disorder-induced "puddles" of electrons, and gate leakage are neglected. Furthermore the contributions of higher order terms on V and I can no longer be neglected in (Eq.6 and 7). The second important operation point is the saturation point where $\lambda=1$ causing $\delta V_0(1)$ to be a maximum yet our equations were derived for linear region only thus we have to revisit them to get the saturation region of operation. However, we can notice that increasing the driving current towards saturation enhances the responsivity of the FET channel.

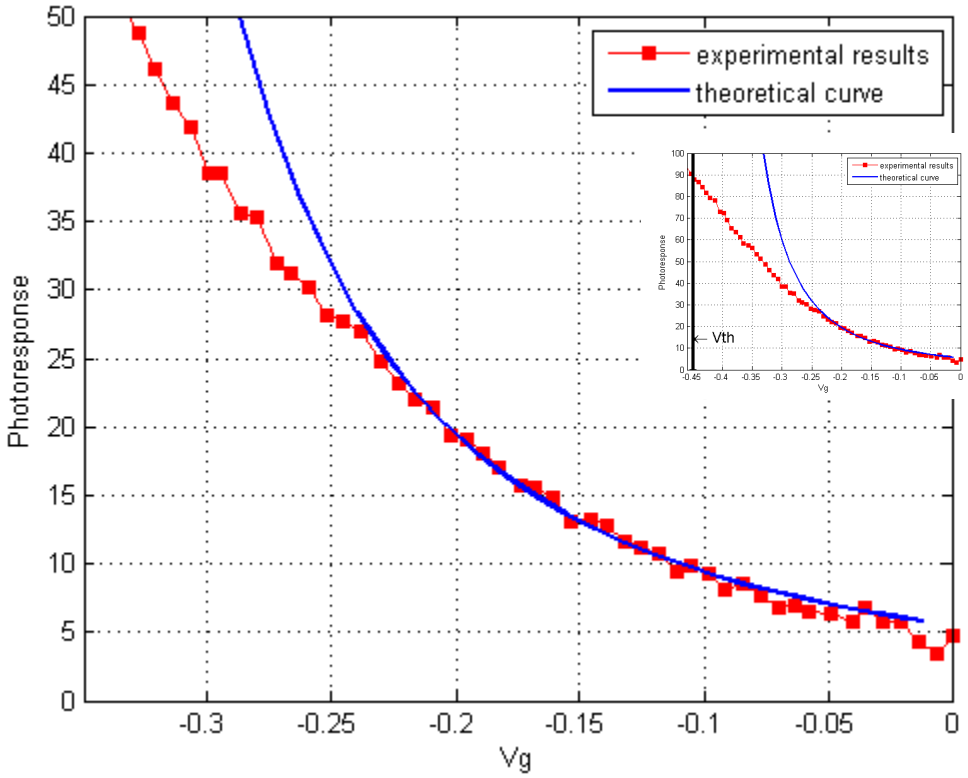

Fig. 3 Photoresponse of THz detection in FET in linear region of operation versus changing gate potential for constant drain potential (V_{ds}=0.1v) using the formula in Eq. 26 (solid line) and the experimental results (squares) from [18]. Inset: the same graph extended to show the photoresponse near the threshold potential (V_{th}=-0.45)

Small signal coupling parameters

The characteristic impedance isn't constant anymore as in the case of uniform transmission lines. However we are only interested in the input impedance since it defines the coupling between the incident signal and active input AC signal. To get the input impedance we start from the input current

$$h_1(0) = -\frac{V_{gs0}V_{gs1}}{L}\left\{\frac{-\lambda}{8} - \frac{\sqrt{i}}{\varepsilon}\right\}$$

And for $\varepsilon \ll 1$

$$h_1(0) = V_{gs0}V_{gs1}\frac{\sqrt{i}}{\varepsilon L} \qquad 30$$

The input impedance is:

$$Z(0) = \frac{V_1(0)}{\mu c h_1(0)} = \frac{V_{g1}L}{V_{gs0}V_{gs1}\mu c\left(\frac{\sqrt{i}}{\varepsilon}\right)} = \frac{L\varepsilon}{V_{gs0}\mu c\sqrt{i}}$$

The input admittance

$$Y(0) = \sqrt{i}\frac{\mu c V_{gs0}}{L\varepsilon} = \sqrt{i\omega\mu c V_{gs0}} = \sqrt{\frac{i\omega c}{r(0)}} \qquad 31$$

Where $r(0)$ is the input DC resistance or the resistance at x=0 and $V_1(0)=V_{gs0}$. The result above is similar to the results in [15] thus we can expect to have the same power coupling efficiency

$$\xi = |\xi_V(\omega)|^2 = \frac{1}{\left(1+\sqrt{\omega/(2\omega_{RO})}\right)^2 + \left(\sqrt{\omega/(2\omega_{RO})}\right)^2} \qquad 32$$

Where ω_{RO} is the roll of frequency $\omega_{RO}^{-1} = 2\pi(R_{acc} + R_A)\times\mu c\, V_{gs0}$, R_{acc} is the access resistance and R_A is the antenna impedance (assuming antenna is operating at resonance frequency such that the impedance is real only). And for high frequency we get

$$\xi_V(\omega) \cong \frac{1}{1+\omega/\omega_{RO}} \qquad 33$$

where ξ_V in the biasing efficiency between the incident signal and the active bias on the FET channel.

Comparing the results in (Eq. 32) to the results in ref. [15] shows that our model includes both the frequency dependence as well as the external bias dependence (V_{gs}). According to (Eq. 32) the roll off frequency is dependent on gate DC bias, such that approaching the threshold voltage ($V_{gs0}>V_{th}$ for linear operation or $V_{gs0}=(V_{gs0}- V_{th})>0$) gives a maximum frequency performance due to the maximized input impedance [15].

Conclusion

This work has proposed a model to represent the channel of a linear FET in non-resonant THz detection regime based on a non-quasi static, nonlinear Transmission line model. Where the characteristic parameters are derived directly from the differential equation of the FET channel. The equations are solved analytically and the rectified output, as well as some basic parameters of operation, and the coupling efficiency are derived. A comparison with previously published experimental results shows good agreement away from the threshold limit.

References

1. Lu, J.-Q., Shur, M.S., Hesler, J.L., Sun, L., Weikle, R.: Terahertz detector utilizing two-dimensional electronic fluid. IEEE Electron Device Letters. 19, 373–375 (1998).
2. Knap, W., Dyakonov, M., Coquillat, D., Teppe, F., Dyakonova, N., Łusakowski, J., Karpierz, K., Sakowicz, M., Valusis, G., Seliuta, D., Kasalynas, I., Fatimy, A.E., Meziani, Y.M., Otsuji, T.: Field Effect Transistors for Terahertz Detection: Physics and First Imaging Applications. J Infrared Milli Terahz Waves. 30, 1319–1337

(2009).
3. Dyer, G.C., Vinh, N.Q., Allen, S.J., Aizin, G.R., Mikalopas, J., Reno, J.L., Shaner, E.A.: A terahertz plasmon cavity detector. Applied Physics Letters. 97, 193507–193507–3 (2010).
4. El Fatimy, A., Teppe, F., Dyakonova, N., Knap, W., Seliuta, D., Valušis, G., Shchepetov, A., Roelens, Y., Bollaert, S., Cappy, A., Rumyantsev, S.: Resonant and voltage-tunable terahertz detection in InGaAs/InP nanometer transistors. Applied Physics Letters. 89, 131926–131926–3 (2006).
5. Teppe, F., Knap, W., Veksler, D., Shur, M.S., Dmitriev, A.P., Kachorovskii, V.Y., Rumyantsev, S.: Room-temperature plasma waves resonant detection of sub-terahertz radiation by nanometer field-effect transistor. Applied Physics Letters. 87, 052107–052107–3 (2005).
6. Knap, W., Kachorovskii, V., Deng, Y., Rumyantsev, S., Lü, J.-Q., Gaska, R., Shur, M.S., Simin, G., Hu, X., Khan, M.A., Saylor, C.A., Brunel, L.C.: Nonresonant detection of terahertz radiation in field effect transistors. Journal of Applied Physics. 91, 9346–9353 (2002).
7. Fatimy, A.E., Tombet, S.B., Teppe, F., Knap, W., Veksler, D.B., Rumyantsev, S., Shur, M.S., Pala, N., Gaska, R., Fareed, Q., Hu, X., Seliuta, D., Valusis, G., Gaquiere, C., Theron, D., Cappy, A.: Terahertz detection by GaN/AlGaN transistors. Electronics Letters. 42, 1342–1343 (2006).
8. Lü, J.-Q., Shur, M.S.: Terahertz detection by high-electron-mobility transistor: Enhancement by drain bias. Applied Physics Letters. 78, 2587–2588 (2001).
9. Tauk, R., Teppe, F., Boubanga, S., Coquillat, D., Knap, W., Meziani, Y.M., Gallon, C., Boeuf, F., Skotnicki, T., Fenouillet-Beranger, C., Maude, D.K., Rumyantsev, S., Shur, M.S.: Plasma wave detection of terahertz radiation by silicon field effects transistors: Responsivity and noise equivalent power. Applied Physics Letters. 89, 253511–253511–3 (2006).
10. Lisauskas, A., Von Spiegel, W., Boubanga-Tombet, S., El Fatimy, A., Coquillat, D., Teppe, F., Dyakonova, N., Knap, W., Roskos, H.G.: Terahertz imaging with GaAS field-effect transistors. Electronics Letters. 44, 408–409 (2008).
11. Lisauskas, A., Pfeiffer, U., Öjefors, E., Bolìvar, P.H., Glaab, D., Roskos, H.G.: Rational design of high-responsivity detectors of terahertz radiation based on distributed self-mixing in silicon field-effect transistors. Journal of Applied Physics. 105, 114511–114511–7 (2009).
12. Ojefors, E., Baktash, N., Zhao, Y., Hadi, R.A., Sherry, H., Pfeiffer, U.R.: Terahertz imaging detectors in a 65-nm CMOS SOI technology. ESSCIRC, 2010 Proceedings of the. pp. 486–489 (2010).
13. Ojefors, E., Pfeiffer, U.R., Lisauskas, A., Roskos, H.G.: A 0.65 THz Focal-Plane Array in a Quarter-Micron CMOS Process Technology. IEEE Journal of Solid-State Circuits. 44, 1968–1976 (2009).
14. Lee, Shur, M.: Semiconductor Device Modeling for VLSI. Prentice Hall PTR (1993).
15. Preu, S., Kim, S., Verma, R., Burke, P.G., Sherwin, M.S., Gossard, A.C.: An improved model for non-resonant terahertz detection in field-effect transistors. Journal of Applied Physics. 111, 024502–024502–9 (2012).
16. Veksler, D., Teppe, F., Dmitriev, A.P., Kachorovskii, V.Y., Knap, W., Shur, M.S.: Detection of terahertz radiation in gated two-dimensional structures governed by dc current. Phys. Rev. B. 73, 125328 (2006).
17. Knap, W., Nadar, S., Videlier, H., Boubanga-Tombet, S., Coquillat, D., Dyakonova, N., Teppe, F., Karpierz, K., Łusakowski, J., Sakowicz, M., Kasalynas, I., Seliuta, D., Valusis, G., Otsuji, T., Meziani, Y., Fatimy, A.E., Vandenbrouk, S., Madjour, K., Théron, D., Gaquière, C.: Field Effect Transistors for Terahertz Detection and Emission. J Infrared Milli Terahz Waves. 32, 618–628 (2011).
18. Nadar, S., Videlier, H., Coquillat, D., Teppe, F., Sakowicz, M., Dyakonova, N., Knap, W., Seliuta, D., Kašalynas, I., Valušis, G.: Room temperature imaging at 1.63 and 2.54 THz with field effect transistor detectors. Journal of Applied Physics. 108, 054508–054508–5 (2010).